Bundschuh or not Bundschuh? Discussing criteria defining the Bundschuh Nappe in the light of new P-T-t data from two localities in the Gurktal Alps (Upper Austroalpine Unit, Eastern Alps)

MARIANNE SOPHIE HOLLINETZ[1], MANUEL WERDENICH[1], CHRISTOPH IGLSEDER[2], BENJAMIN HUET[2], MARTIN REISER[2], RALF SCHUSTER[2], PETER TROPPER[3], GERD RANTITSCH[4] & BERNHARD GRASEMANN[1]

[1] University of Vienna, Department of Geodynamics and Sedimentology, Althanstraße 14, 1090 Vienna. marianne.sophie.hollinetz@univie.ac.at; manuel.werdenich@gmx.at; bernhard.grasemann@univie.ac.at
[2] Geological Survey of Austria, Department of Hard-Rock Geology, Neulinggasse 38, 1030 Vienna. christoph.iglseder@geologie.ac.at; benjamin.huet@geologie.ac.at; martin.reiser@geologie.ac.at; ralf.schuster@geologie.ac.at
[3] University of Innsbruck, Department of Mineralogie and Petrology, Innrain 52, 6020 Innsbruck. peter.tropper@uibk.ac.at
[4] University of Leoben, Department of Applied Geosciences and Geophysics, Peter-Tunner-Straße 5, 8700 Leoben. gerd.rantitsch@unileoben.ac.at

1. Introduction

In the Eastern Alps, the Upper Austroalpine Unit represents a nappe stack that received its pervasive tectono-metamorphic imprint during the Eo-Alpine event in the Cretaceous (Text-Fig. 1a; SCHMID et al., 2004; FROITZHEIM et al., 2008). This nappe stack consists of a polymetamorphic basement, Paleozoic metasediments and a partly metamorphosed Permian to Mesozoic cover. Nappes dominated by Paleozoic metasediments and basement rocks are grouped into four nappe systems. From bottom to the top, these are the Silvretta-Seckau, Koralpe-Wölz, Ötztal-Bundschuh and Drauzug-Gurktal Nappe Systems. Except the Koralpe-Wölz Nappe System, all of them contain Permomesozoic cover sequences, which were originally used for the tectonic subdivision (TOLLMANN, 1963, 1977). Where this cover is absent or extremely thinned, identifying the exact position of the tectonic contact separating the nappe systems becomes complicated. In this case, a detailed characterization of the tectono-metamorphic imprint and its kinematics during the pre-Alpine and Eo-Alpine events is crucial.
In the Gurktal Alps (Styria and Carinthia), the Koralpe-Wölz Nappe System is represented by the Gstoder Nappe, mainly built up by monophase metamorphic micaschist of the Radenthein Complex (IGLSEDER & HUET, 2019). Above it, the Bundschuh Nappe of the Ötztal-Bundschuh Nappe System contains the Bundschuh-Priedröf Complex which corresponds to a pre-Permian basement unit, as well as a Permian to Mesozoic cover sequence ('Stangalm Mesozoic', STOWASSER, 1956; PISTOTNIK, 1974). The crystalline basement consists of intercalated garnet-bearing paragneiss and micaschist, hosting orthogneiss of Middle Ordovician protolith age (Bundschuh Orthogneiss Lithodem). Two-phased garnets indicate at least lower amphibolite-facies metamorphism during both the Variscan and the Eo-Alpine events (SCHUSTER, 1994; SCHUSTER & FRANK, 1999; KOROKNAI et al., 1999). Towards the top of the Bundschuh Nappe, the metamorphic temperature related to the Eo-Alpine event decreases to ~450° C (e.g. SCHUSTER, 2015). The Bundschuh Nappe is tectonically overlain by the Murau and Königstuhl nappes which belong to the Drauzug-Gurktal Nappe System (Text-Fig. 1b). As an exception, in the Oberhof Window the Gstoder Nappe from the Koralpe-Wölz Nappe System is intercalated between the Bundschuh and the Murau nappes (HOLLINETZ, 2018). In this contribution, we present petrological and geochronological data from two representative samples of rock units, which occur along the boundaries between the above mentioned nappes and which do not have a clear tectonic position: (1) a garnet- and chloritoid-bearing micaschist sampled below the NW-margin of the Murau Nappe in the vicinity of Stadl an der Mur and (2) a garnet-chloritoid-bearing graphite schist sampled in the Oberhof Window (Text-Fig. 1b).

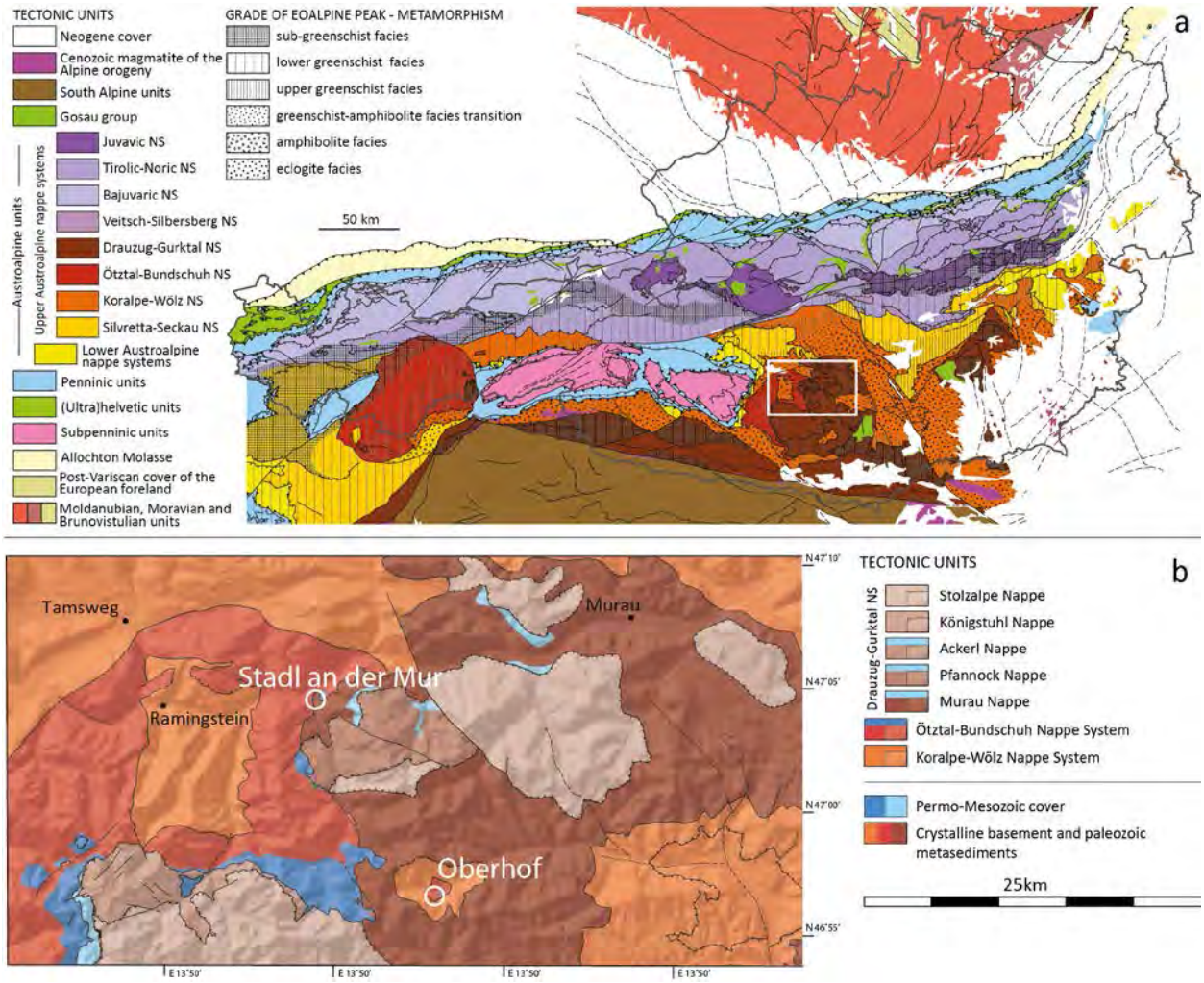

Text-Fig. 1: a) Tectonic and metamorphic overview map of the Eastern Alps (modifed after SCHUSTER, 2015). b) Tectonic map of the Gurktal Alps with location of the studied samples.

2. Structural and petrological analysis

2.1. Locality Stadl an der Mur (Styria)

In the Southeast of the village Stadl an der Mur (UTM33 0423139, 5213269, see Text-Fig. 1b) a garnet-bearing and partly graphitic micaschist is exposed structurally below several tens of meters of quartzite. This quartzite is expected to be Early Triassic in age and might be interpreted as a continuation of the Stangalm Mesozoic, representing the top of the Bundschuh Nappe. The quartzite is overlain by the basal parts of the Murau Nappe (FRIMMEL, 1987). The rocks show a strong internal variability with respect to their quartz versus white mica content. Abundant garnets reach sizes of 7 mm and appear macroscopically two-phased (Text-Fig. 2a). Two sets of foliations where identified. The older foliation defining the metamorphic layering is isoclinally to tightly folded by NE–SW to E–W trending fold axes. It is overprinted by a younger crenulation cleavage parallel to the fold axial surface that shallowly dips to the North. Thin section observation of garnet inclusion trails indicates that garnet grew syntectonically with respect to folding (Text-Fig. 2b). Macroscopically, C'-type shear bands overprinting the crenulation cleavage with an E–W trending striation were observed. Stepping of quartz fibres indicates top-to-the-E kinematics, which is in agreement with the C'-type fabric and the crystallographic preferred orientation (CPO) in monomineralic quartz layers observed in thin section.

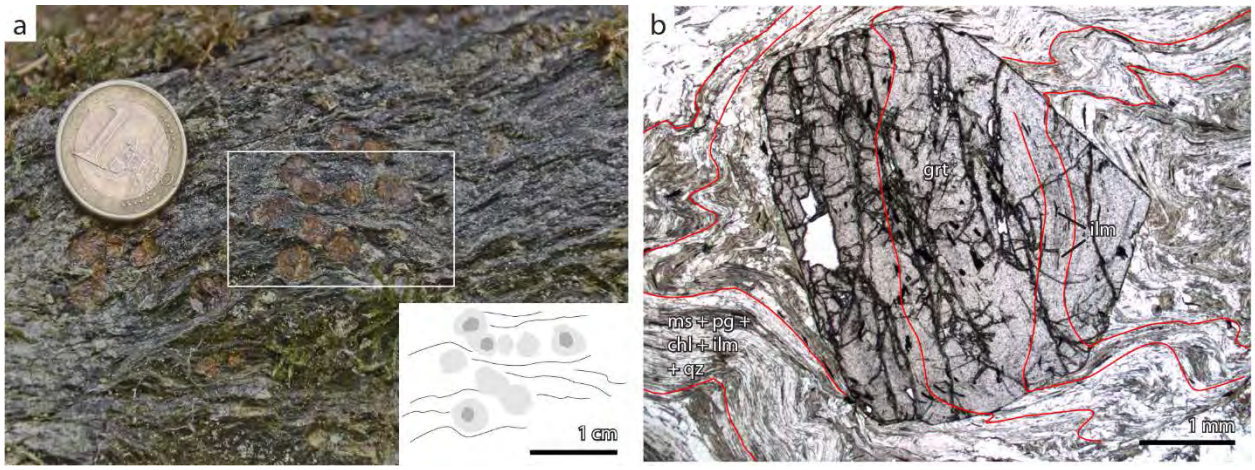

Text-Fig. 2: a) Garnet-bearing micaschist with garnets appearing macroscopically two-phased with a darker core and a brighter rim (UTM33 0423079, 5213293). b) Photomicrograph of garnet overgrowing an openly folded foliation delineated by aligned ilmenite and graphite. Folding continued after garnet growth ceased.

Petrographic characterization using scanning electron microscopy revealed a matrix consisting of chlorite, muscovite, paragonite, ilmenite and quartz (Text-Fig. 3a). Subordinate biotite and plagioclase were observed; the latter is restricted to late-stage cracks at a high angle with respect to the foliation. Large garnet porphyroblasts define a lepidoplastic microstructure. The apparent core-rim zoning of garnet observed in hand specimen scale was not confirmed at microscopic scale. Conversely, electron microprobe analysis (EMPA) shows that garnet is chemically rather homogeneous with the Mn-content decreasing towards the rim indicating prograde zoning (Text-Fig. 3c). Chloritoid is found both in the matrix and as inclusions in garnet. Allanite, monazite, zircon, apatite and tourmaline occur as accessory minerals in the matrix and as inclusions. Based on microstructural criteria (e.g. straight phase boundaries) the equilibrium assemblage stable at metamorphic peak conditions is considered to be garnet + chloritoid + chlorite + muscovite + paragonite + ilmenite + quartz. Pseudosection modelling using the software Theriak-Domino (DE CAPITANI & PETRAKAKIS, 2010) using a bulk composition derived from whole rock analysis reproduces this assemblage in a narrow P-T field in the range 500–550° C and 8–11 kbar (Text-Fig. 3e). Garnet isopleths corresponding to the rim composition are parallel to each other and crosscut this field at approximately 530° C and 10 kbar. These P-T conditions are considered to reflect the peak of metamorphism and are consistent with a maximum temperature of 520 ± 30° C determined by Raman microspectroscopy of carbonaceous material (RANTITSCH et al., in prep.).

2.2. Locality Oberhof (Carinthia)

In the core of the Oberhof Window an association of a garnet- and chloritoid-bearing graphite-schist, quartzite and a dolomite marble is exposed structurally above an orthogneiss. This orthogneiss is of Middle Ordovician protolith age (HOLLINETZ, 2018) and belongs to the Bundschuh Orthogneiss Lithodem of the Bundschuh Nappe. Due to its lithological composition, the graphite-schist is thought to represent a higher metamorphic grade equivalent of Pennsylvanian (late Carboniferous) metasediments of the anchizonal Königstuhl Nappe (HAIGES 1984). However, it may also belong the Gstoder Nappe, since typical garnet and hornblende-bearing micaschist of the Radenthein Complex occurs nearby.

The graphite-schist shows a pronounced metamorphic layering reflected by the abundance and size of porphyroblasts (mostly garnet and chloritoid) parallel to the penetrative schistosity. Both are tightly folded with NE–SW trending fold axes and subhorizontal axial surfaces. In the quartzite overlying the graphite schist strongly developed shape preferred orientation (SPO) and CPO of quartz indicates top-to-the-E shearing. A graphite-schist sample was collected at UTM33 432826, 5199569 (Text-Fig. 1b). Garnet is usually smaller than 3 mm (Text-Fig. 3b). Chloritoid occurs abundantly subparallel to the schistosity and partly as inclusions in garnet, whereas chlorite forms large (~5 mm) porphyroblasts oblique to the schistosity. The matrix consists of muscovite, quartz, ilmenite and graphite. Apatite, monazite and zircon occur as accessory minerals. Ilmenite and graphite inclusion trails in garnet indicate that garnet overgrew a partly folded foliation.

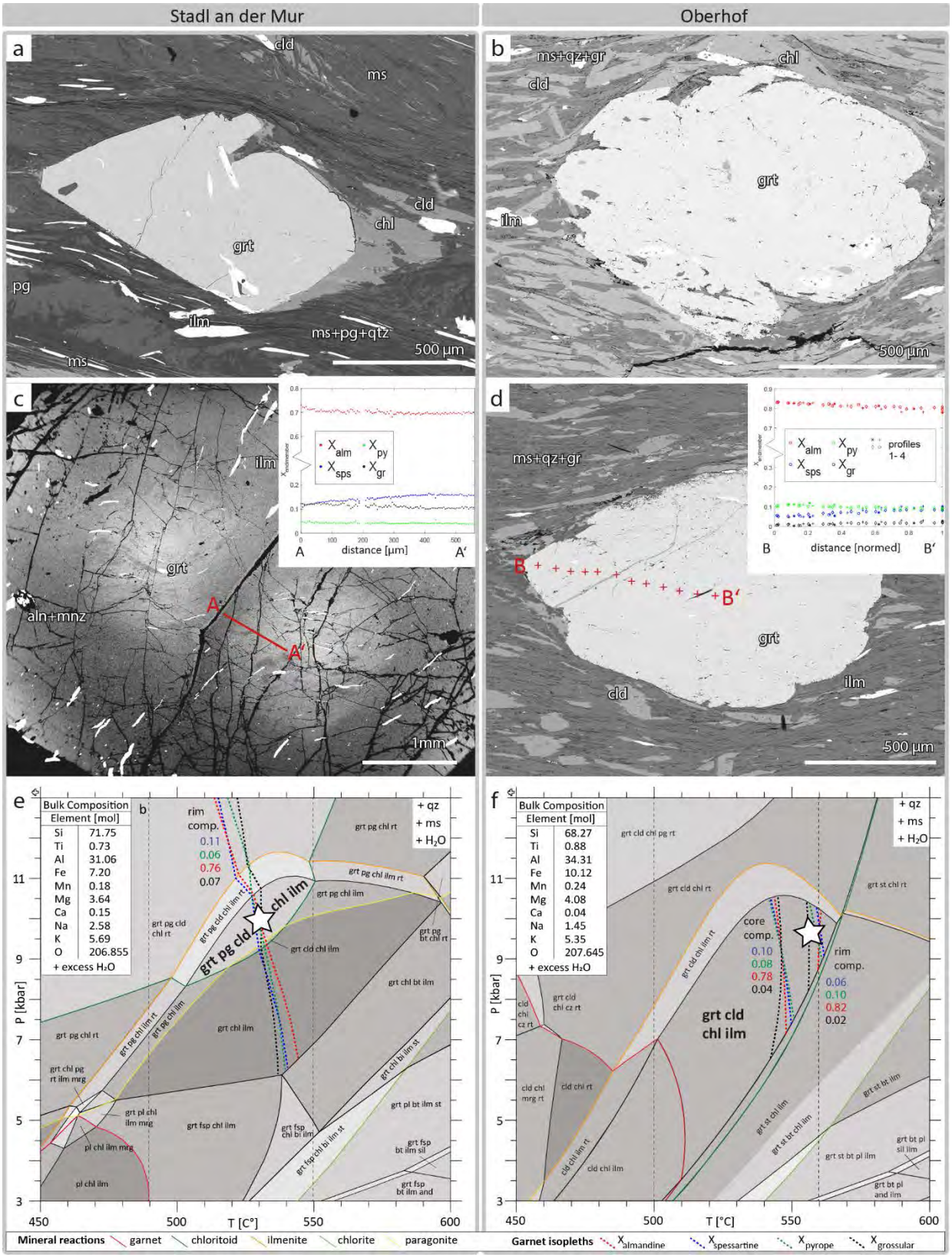

Text-Fig. 3: Petrographic observations and pseudosection modelling of samples from Stadl an der Mur (left column) and Oberhof (right column). a, b) Representative BSE images showing the mineral assemblage assumed to be stable at peak metamorphic conditions. c, d) BSE images of garnet and corresponding chemical composition along a profile. The profile in d summarizes data from four different garnets. e, f) Pseudosections calculated from the bulk composition given in the upper left corner. Calculations were performed with the Theriak-Domino software (De Capitani & Petrakakis, 2010) package using the thermodynamic database of Holland & Powell (2011) and the activity-composition relations of White et al. (2014a, b). The white star marks the interpreted peak P-T conditions, vertical dashed black lines give the uncertainty interval of the peak T obtained by Raman microspectroscopy of carbonaceous material (Rantitsch et al., in prep.). Mineral abbreviations according to Whitney & Evans (2010).

Chemically, garnets show a continuous zoning with a decreasing Mn-content towards the rim and a very low Ca-content (Text-Fig. 3d). Based on microstructural criteria, the metamorphic peak assemblage is considered to be garnet + chloritoid + chlorite + muscovite + ilmenite + quartz.
A pseudosection calculated with the bulk rock composition of the sample shows that this assemblage is stable in a wide P-T field spreading over 510–560° C and 4–10 kbar. This field is crossed by the garnet isopleths corresponding to the measured rim composition close to its upper end at approximately 560° C and 9 kbar, which is considered to reflect the peak metamorphic conditions (Text-Fig. 3f). The maximum temperatures determined by Raman microspectroscopy of carbonaceous material is slightly lower at 530 ± 30° C, but agrees within error (RANTITSCH et al., in prep.).

3. U-Th-Pb monazite geochronology

Monazite is an abundant accessory mineral occurring in both studied samples. Monazite grains were carefully characterized using SEM imaging and measured with a JEOL 8100 SUPERPROBE electron microprobe at the Institute of Mineralogy and Petrography (University of Innsbruck/Austria) in order to determine the U-Th-Pb ages of metamorphism. The instrument was operated following the approach described in THÖNI et al. (2008), using 15 kV accelerating potential and a beam current of 10 nA. Counting times were set to 40 sec. for both peak and background for the major elements, 40/40 sec. (peak/background) for Th, 200/150 sec. for trace elements and 300/200 sec. for U and Pb.

3.1. Locality Stadl an der Mur

Monazite commonly forms either aggregates of several grains together with chlorite and remnants of allanite or occurs in close vicinity of partially resorbed allanite (Text-Fig. 4a, e). Additionally, it is found as individual grains in the matrix or replacing inclusionary allanite in garnet along chlorite-filled cracks (Text-Fig. 4i). High contrast BSE images reveal compositional zoning of some grains with Th-rich monazite appearing bright (Text-Fig. 4f). For most cases, it is interpreted that monazites forms from the prograde breakdown of allanite at lower amphibolite facies conditions (SPEAR, 2010). Conversely, monazite replacing allanite inclusions in garnet is interpreted to have formed from the retrograde breakdown of allanite (Text-Fig. 4i, j, k).
Most calculated U-Th-Pb ages range between 63 ± 19 Ma and 161 ± 41 Ma (Text-Fig. 4b, f, n). Th/U ratios show a large range of 2–35 with no correlation to calculated ages or microstructural relations. The Yttrium content of most grains varies between 0.4 and 1 mol%. Individual grains in the matrix show a lower Yttrium content of ~0.2 mol%, indicating monazite growth after garnet fractionated most of the bulk Yttrium (REISER et al., 2019). However, no unambiguous correlation between microstructural position, monazite chemistry and age was found. A few older ages in the range of 200–500 Ma were obtained from monazites that clearly formed from the breakdown of allanite (e.g. Text-Fig. 4j, k). It is assumed in this case that monazite inherited common lead from its precursor mineral. The incorporation of common lead considerably shifted monazite ages resulting in apparent older ages. Alternatively, the older ages could also be interpreted as partially reset ages of either detrital or metamorphic monazites that formed during pre-alpine (Variscan?) metamorphism. However, due to the absence of a clearly defined older age population or morphologies of monazites indicating a detrital origin, the former hypothesis seems more plausible. For the mean age calculation that resulted in 86 ± 11 Ma (34 analyses, Text-Fig. 4n, o), only analyses that can be texturally clearly correlated to common lead contamination were excluded (Text-Fig. 4i, j, k).
Several interpretations are possible for the set of younger ages. On the one hand, the wide age range would only reflect the large uncertainty of U-Th-Pb microprobe ages and the age data could correspond to a short event in the range 86 ± 11 Ma. On the other hand, the wide age range could also reflect protracted crystallisation of monazite during a time span of possibly 50 million years. In addition, complex chemical processes involving fluid influx and/or common lead might also have an influence. Irrespective of the interpretation, these age data indicate the Cretaceous crystallisation of monazite. This unambiguously shows that the metamorphism recorded in the sample from Stadl an der Mur is Eo-Alpine.

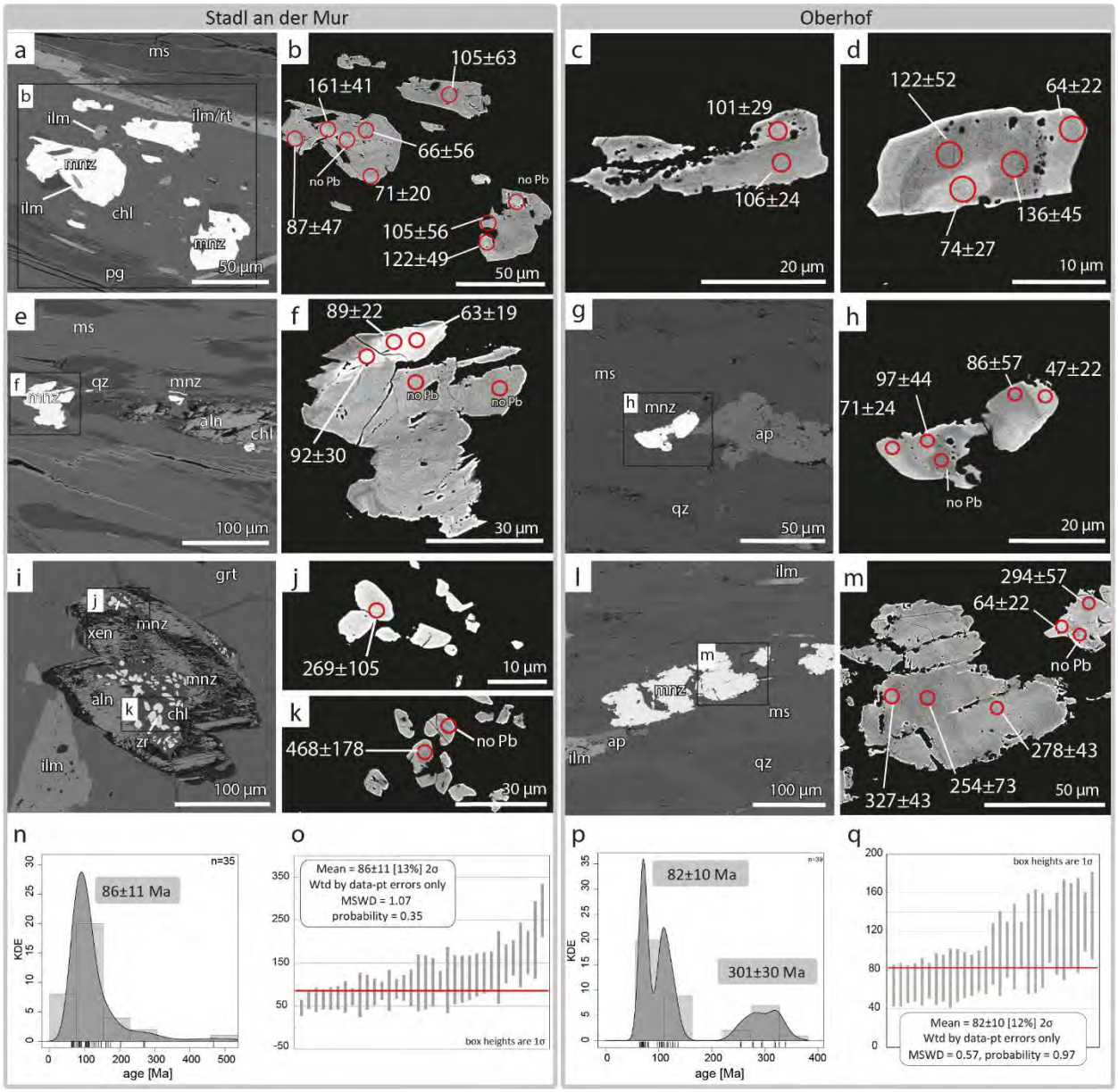

Text-Fig. 4: Monazite data from Stadl an der Mur (left column) and Oberhof (right column). a–m) BSE images of monazites. b, c, d, f, h, j, k, m) High contrast BSE images with date (Ma) and position of the U-Th-Pb microprobe analyses. n, p) Kernel density estimate diagrams (drawn with IsoplotR, VERMEESCH, 2018). Mean ages in grey boxes are given with a 2σ interval. o, q) Weighted mean ages for the young monazite set at 86 ± 11 Ma for the Stadl an der Mur and 82 ± 10 Ma for Oberhof, respectively (drawn with Isoplot 4.15; LUDWIG, 2012).

3.2. Locality Oberhof

In the graphite schist, monazite occurs ubiquitously in the matrix and as inclusions in all porphyroblasts. The grains are rounded to subidiomorphic and commonly smaller than 20 µm. Most grains exhibit distinctive compositional zoning with cores overgrown by one or two rims (Text-Fig. 4c, d). Occasionally, neighbouring U-Th bearing minerals (e.g. apatite, zircon) lead to more complex compositional zoning patterns (Text-Fig. 4g, h). A different, rarely occurring microstructural type of monazite comprises much larger (up to 100 µm) grains with patchy zoning (Text-Fig. 4l, m). These large grains are cracked and thus partly resorbed.

Calculated U-Th-Pb ages for the small, zoned grains range between 47 ± 22 and 136 ± 45 (Text-Fig. 4d, p). Th/U ratios show two populations with most analyses plotting between 1–5 and few grains showing a large range of 6–19, but no correlation with ages or microstructural position can be made so far. In terms of Yttrium-content, most analyses range between 0.5–1.2 mol%. A low-Yttrium monazite population containing 0.1–0.3 mol% Yttrium yields ages around ~65–75 Ma, this population is interpreted to have grown after garnet fractionation. On a kernel density plot

(VERMEESCH, 2018) two sub-peaks are observed (Text-Fig. 4p), but they overlap within error. They are thus treated as representing only one age population. Additionally, sub-grains observed in BSE images exhibit age domains, which are not always consistent with a core-rim morphology (Text-Fig. 4d). Analyses obtained from the zoned grains give a mean age of 82 ± 10 Ma (15 grains, 29 analyses). The same interpretations as for the locality Stadl an der Mur are possible for the sample of Oberhof. However, evidence for Eo-Alpine metamorphism is also here unambiguous.
Two large grains with patchy chemical zoning were analysed (Text-Fig. 4l). Ages obtained from these grains are significantly older and range between 250 and 350 Ma with a mean age at 301 ± 30 Ma (10 analyses). Overgrowth yielding younger ages were also measured (Text-Fig. 4m). Due to the different morphology and the significantly different age, these grains are interpreted as of detrital origin and can probably be related to the Variscan Event. The large spread of the older age population might be explained by alteration of probably Carboniferous ages due to dissolution-precipitation processes during fluid-dominated Eo-Alpine metamorphism. In this sample, monazite-growth cannot be correlated to the breakdown reaction of a precursor mineral. Instead, Eo-Alpine metamorphic monazite is assumed to have crystallized from detrital monazite via a dissolution-precipitation mechanism.

4. Discussion

Summarizing data from the studied localities Stadl an der Mur and Oberhof, the following similarities are noted:

(1) There is no unambiguous evidence of Mesozoic cover at the upper boundary of the Bundschuh Nappe in the investigated area, even though the thick quartzite in Stadl an der Mur can be considered as Permian or Lower Triassic and the dolomite in Oberhof could be considered as a metamorphic equivalent of the Weißwände Lithodem (HOLLINETZ, 2018).
(2) Raman microspectroscopy of carbonaceous material and pseudosection modelling consistently yield 530–560° C and 9–10 kbar for metamorphic peak P-T conditions.
(3) Monazite U-Th-Pb microprobe ages allow unambigous assignment of the metamorphic imprint to the Eo-Alpine event. In case the age data reflect a single growth event, the ages from both localities (86 ± 11 Ma for the Stadl an der Mur and 82 ± 10 Ma for Oberhof) overlap within uncertainty. No earlier tectono-metamorphic event could be unambiguously identified. The older measured ages are interpreted to reflect either common lead contamination from allanite or stem from detrital grains.
(4) During the earlier stage of exhumation, the rocks deformed by folding. Top-to-the-E shearing accommodated exhumation from greenschist facies conditions to the brittle-ductile transition.

Comparing the monazite age data of both localities, the most striking difference is that only one monazite population was identified in the Stadl an der Mur sample, whereas data from Oberhof might indicate two populations. Bearing in mind the large errors of the single ages and the strong age dispersion, it remains questionable whether the calculated mean ages are geologically meaningful. Reasons for the strong dispersion of the ages could relate to inherited lead from allanite (in the sample from Stadl an der Mur) or complex fluid/rock interaction as inferred from partly peculiar zoning patterns (sample from Oberhof). Nonetheless, the data unambiguously verify the Eo-Alpine age of the metamorphism for both localities.
Diagnostic elements of the Bundschuh Nappe as it is currently defined comprise (1) two-phase garnets that record at least lower amphibolite facies conditions for both the Variscan and the Eo-Alpine Event in the Bundschuh-Priedröf Complex, (2) the occurrence of orthogneiss of Ordovician intrusion age and (3) the presence of a Permomesozoic cover sequence (SCHUSTER, 2015 and references therein). Garnet-bearing micaschist showing solely an Eo-Alpine imprint as both samples of this study do is thus rather untypical.
If considered as a part of the Bundschuh Nappe, the samples cannot be part of the Bundschuh-Priedröf Complex due to the lack of a Variscan metamorphic imprint. Thus, these lithologies must

be part of a post-Variscan cover sequence, which might already have commenced in the Pennsylvanian. So far, Carboniferous metasediments have not been described in the Bundschuh Nappe, but are known from the lower metamorphic nappes of the Drauzug-Gurktal Nappe System (Stangnock Formation, KRAINER, 1989; HUET, 2015). It is reasonable to argue that possible Carboniferous metasediments in the Bundschuh Nappe have not been recognized as such since once overprinted and deformed at upper greenschist facies conditions during the Eo-Alpine Event, they might be macroscopically indistinguishable from the crystalline basement. However, this would be only the case for a pelitic protolith, whereas the Stangnock Formation is characterized by fluvial sediments comprising conglomerates, sandstones and shales. A criterion to identify post-Variscan lithologies would be detrital monazites of Variscan ages.
An alternative interpretation explaining the P-T-t data of both localities is to assign the samples to a tectonic unit that is not the Bundschuh Nappe. The structural position of the sample from Oberhof would allow assignment to the Gstoder Nappe (Koralpe-Wölz Nappe System), whereas the sample from Stadl an der Mur could represent a basal sliver of the Murau Nappe (Drauzug-Gurktal Nappe System).
To clarify ultimately the affiliation of 'transitional lithologies' as in the present study, we highlight the need for more precise P-T-t-D data. If results of this study can be confirmed from other comparable localities, a modification of the lithostratigraphical model to account for post-Variscan (Pennsylvanian to Lower Triassic) siliciclastic metasediments in the Bundschuh Nappe might be envisaged. Finally, we emphasize that modern petrological, geochronological and structural data provide the basis for a consistent tectono-stratigraphy and thus for any geological map.

References

DE CAPITANI, C.D. & PETRAKAKIS, K. (2010): The computation of equilibrium assemblage diagrams with Theriak/Domino software. – American Mineralogist, **95**/7, 1006–1016, Washington, D.C.

FRIMMEL, H.E. (1987): Strukturgeologische, geochemische und geochronologische Untersuchungen zur Entwicklungsgeschichte des NW-Randes der Gurktaler Decke (Oberostalpin). – Dissertation, Universität Wien, 199 S., Wien.

FROITZHEIM, N., PLASIENKA, D. & SCHUSTER, R. (2008): Alpine tectonics of the Alps and Western Carpathians. – The Geology of Central Europe, **2**, 1141–1232, London.

HAIGES, K.-H. (1984): Geologie und Tektonik des Oberhofer Fensters und seiner Umrahmung im Norden der Gurktaler Alpen (Nordkärnten – Österreich). – Dissertation, Universität Hamburg, 254 S., Hamburg.

HOLLAND, T.J.B. & POWELL, R. (2011): An improved and extended internally consistent thermodynamic dataset for phases of petrological interest, involving a new equation of state for solids. – Journal of Metamorphic Geology, **29**/3, 333–383, Oxford.

HOLLINETZ, M.S. (2018): Tectono-metamorphic evolution of the upper part of the Eo-Alpine extrusion wedge. A case study from the Oberhof window (Carinthia, Austria). – Masterarbeit, Universität Wien, 87 S., Wien.

HUET, B. (2015): Strukturgeologie der Stolzalpe-Decke auf Blatt Radenthein-Ost (UTM 3106). – Jahrbuch der Geologischen Bundesanstalt, **155**/1–4, 121–145, Wien.

IGLSEDER, C. & HUET, B. (2019): Tektonische Einheiten auf GK25 Blatt Radenthein-Ost und angrenzenden Gebieten. – In: GRIESMEIER, G.E.U. & IGLSEDER, C. (Eds.): Arbeitstagung 2019 der Geologischen Bundesanstalt. – Geologie des Kartenblattes GK25 Radenthein-Ost (Murau), 5–18, Geologische Bundesanstalt, Wien.

KOROKNAI, B., NEUBAUER, F., GENSER, J. & TOPA, D. (1999): Metamorphic and tectonic evolution of Austroalpine units at the western margin of the Gurktal nappe complex, Eastern Alps. – Schweizerische Mineralogische und Petrographische Mitteilungen, **79**/2, 277–295, Zürich. http://dx.doi.org/10.5169/seals-60209

KRAINER, K. (1989): Die fazielle Entwicklung der Oberkarbonsedimente (Stangnock-Formation) am NW-Rand der Gurktalerdecke. – Carinthia II, **179/99**, 563–601, Klagenfurt.

LUDWIG, K. (2012): User´s manual for Isoplot 3.75–4.15: a geochronological toolkit for Microsoft Excel. – Berkeley Geochronology Center Special Publication, **5**, 75 S., Berkeley, California.

PISTOTNIK, J. (1974): Zur Geologie des NW-Randes der Gurktaler Masse (Stangalm-Mesozoikum, Österreich). – Mitteilungen der Geologischen Gesellschaft in Wien, **66–67**, 127–141, Wien.

RANTITSCH, G., IGLSEDER, C., HOLLINETZ, M.S., HUET, B., SCHUSTER, R. & WERDENICH, M. (in prep.): Organic metamorphism within the Eo-Alpine upper plate (NW margin of the Gurktal Alps, Upper Austroalpine Eastern Alps). – In preparation.

REISER, M.K., SĂBĂU, G., NEGULESCU, E., SCHUSTER, R., TROPPER, P. & FÜGENSCHUH, B. (2019): Post-Variscan metamorphism in the Apuseni and Rodna Mountains (Romania): evidence from Sm–Nd garnet and U–Th–Pb monazite dating. – Swiss Journal of Geosciences, **112**/1, 101–120, Heidelberg.

SCHMID, S.M., FÜGENSCHUH, B., KISSLING, E. & SCHUSTER, R. (2004): Tectonic map and overall architecture of the Alpine orogen. – Eclogae Geologicae Helvetiae, **97**/1, 93–117, Basel.

SCHUSTER, R. (1994): Die alpine Großüberschiebung an der Basis des Bundschuhkristallins. Steiermark/Kärnten/Salzburg. – Diplomarbeit, Universität Wien, 121 S., Wien.

SCHUSTER, R. (2015): Zur Geologie der Ostalpen. – Abhandlungen der Geologischen Bundesanstalt, **64**, 143–165, Wien.

SCHUSTER, R. & FRANK, W. (1999): Metamorphic evolution of the Austroalpine units east of the Tauern Window: indications for Jurassic strike slip tectonics. – Mitteilungen der Gesellschaft der Geologie- und Bergbaustudenten in Österreich, **42**, 37–58, Wien.

SPEAR, F. (2010): Monazite–allanite phase relations in metapelites. – Chemical Geology, **279**, 55–62, Amsterdam.

STOWASSER, H. (1956): Zur Schichtfolge, Verbreitung und Tektonik des Stangalm-Mesozoikums (Gurktaler Alpen). – Jahrbuch der Geologischen Bundesanstalt, **99**, 65–199, Wien.

THÖNI, W.F., TROPPER, P., SCHENNACH, F., KRENN, E., FINGER, F., KAINDL, R. & HOINKES, G. (2008): The metamorphic evolution of migmatites from the Ötztal Complex (Tyrol, Austria) and constraints on the timing of the pre-Variscan high-T event in the Eastern Alps. – Swiss Journal of Geosciences, **101**/1, 111–126, Basel.

TOLLMANN, A. (1963): Ostalpensynthese. – 256 S., Wien (Deuticke).

TOLLMANN, A. (1977): Geologie von Österreich, Band I: Die Zentralalpen, 320–322, Wien (Deuticke).

VERMEESCH, P. (2018): IsoplotR: a free and open toolbox for geochronology. – Geoscience Frontiers, **9**/5, 1479–1493, Amsterdam.

WHITE, R., POWELL, R., HOLLAND, T., JOHNSON, T. & GREEN, E. (2014a): New mineral activity–composition relations for thermodynamic calculations in metapelitic systems. – Journal of Metamorphic Geology, **32**/3, 261–286, Oxford.

WHITE, R., POWELL, R. & JOHNSON, T. (2014b): The effect of Mn on mineral stability in metapelites revisited: New a–x relations for manganese-bearing minerals. – Journal of Metamorphic Geology, **32**/8, 809–828, Oxford.

WHITNEY, D.L. & EVANS, B.W. (2010): Abbreviations for names of rock-forming minerals. – American mineralogist, **95**/1, 185–187, Washington, D.C.